Supplementary Information for

New insights into the structural heterogeneity and geodynamics of the Indo-Burma subduction zone from ambient noise tomography

Shucheng Wu[1,2], Jiayuan Yao[1], Shengji Wei[2,3], Judith Hubbard[2,3], Yu Wang[4], Yin Myo Min Htwe[5], Myo Thant[6], Xin Wang[7], Kai Wang[8], Tianshi Liu[10], Qinya Liu[9,10], Ping Tong[1,3]

[1]Division of Mathematical Sciences, School of Physical and Mathematical Sciences, Nanyang Technological University, Singapore, Singapore.

[2]Earth Observatory of Singapore, Nanyang Technological University, Singapore, Singapore.

[3]Asian School of the Environment, Nanyang Technological University, Singapore, Singapore.

[4]Department of Geosciences, National Taiwan University, Taipei, Taiwan.

[5]Department of Meteorology and Hydrology, Nay Pyi Taw, Myanmar.

[6]Department of Geology, University of Yangon, Yangon, Myanmar.

[7]Seismological Laboratory, California Institute of Technology, Pasadena, CA, USA

[8]Australian Research Council Centre of Excellence for Core to Crust Fluid Systems (CCFS) and GEMOC, Department of Earth and Planetary Sciences, Macquarie University, NSW, Australia.

[9]Department of Physics, University of Toronto, Toronto, Ontario, Canada.

[10]Department of Earth Science, University of Toronto, Toronto, Ontario, Canada.

Correspondence: Ping Tong (tongping@ntu.edu.sg)

Supplementary figures:

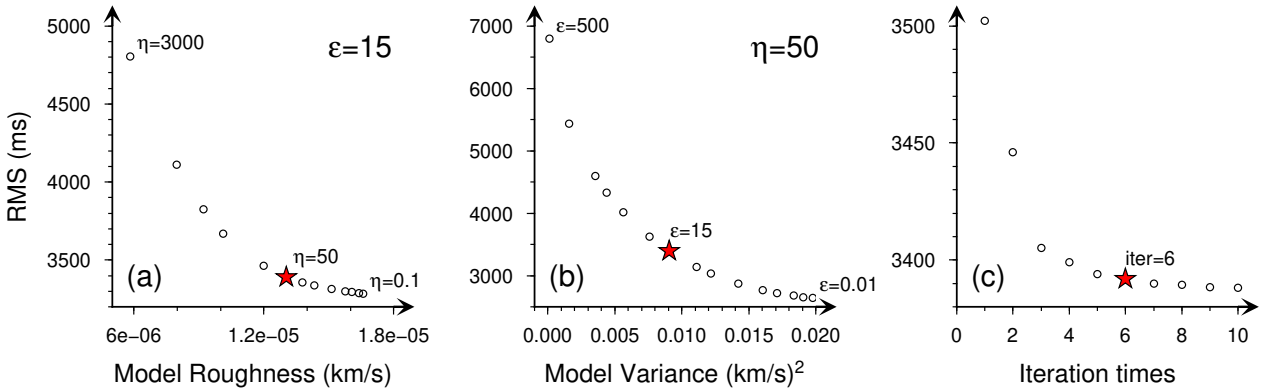

Fig. S1 *L*-curves of RMS misfit versus (a) model roughness, (b) model variance, and (c) iteration times at the period of 20 s. *L*-curve in (a) is calculated by fixing the damping parameter at 15 and varying the smoothing parameter from 0.1 to 3000. *L*-curve in (b) is generated by setting the smoothing parameter to 50 and varying the damping parameter from 0.01 to 500. *L*-curve in (c) is obtained by performing the tomographic inversion for ten iterations with fixed damping and smoothing parameters of 15 and 50, respectively. The red stars denote the choice of parameters in this study.

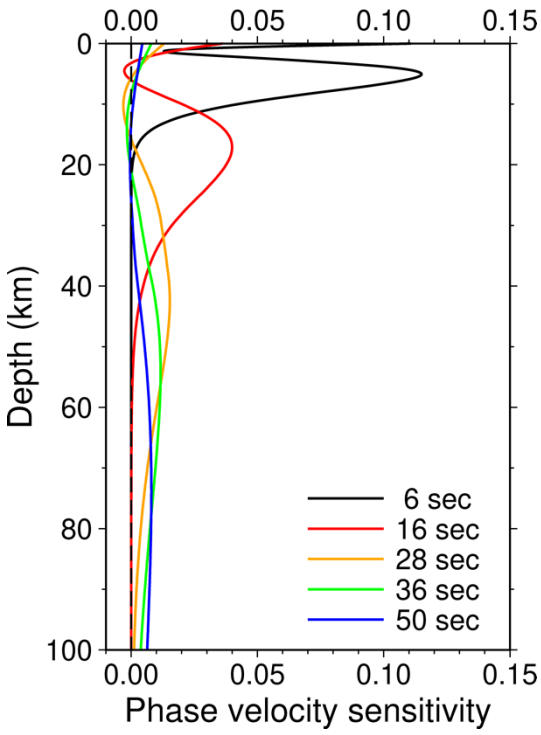

Fig. S2 1-D phase velocity sensitivity kernels calculated based on a regional average model at the periods of 6, 16, 28, 36, and 50 s.

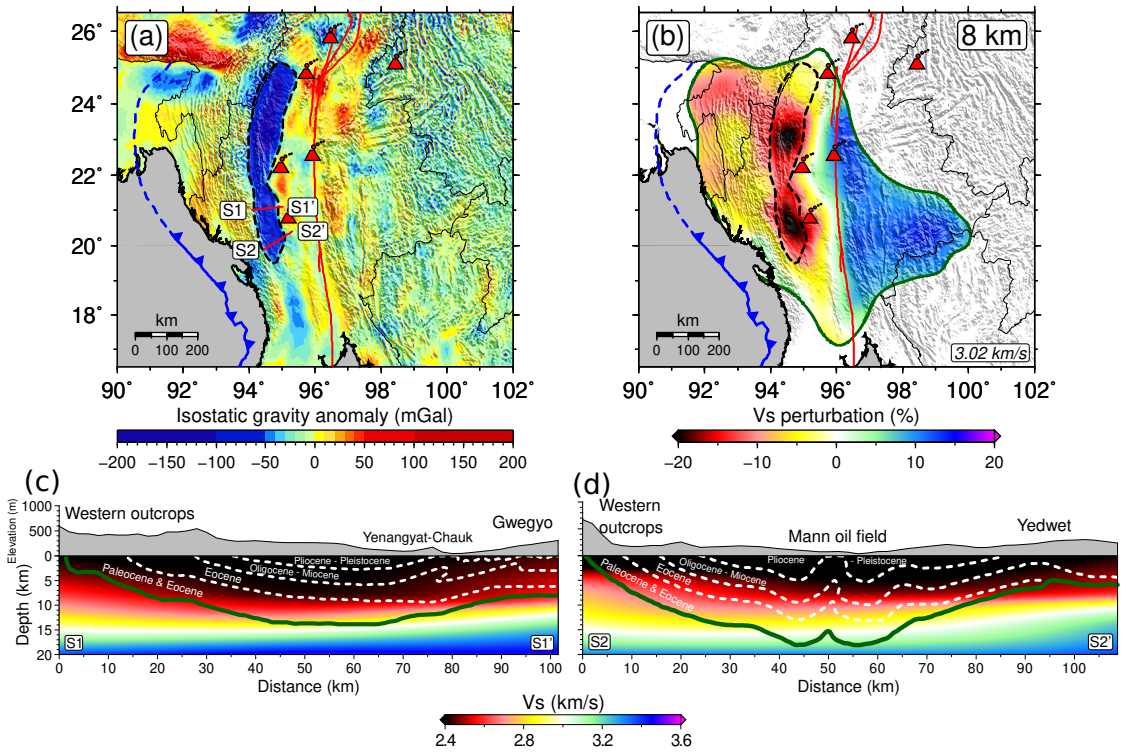

Fig. S3 Comparison between our inverted shear-wave velocity model, isostatic gravity anomaly, and the oil prospecting profiles. (a) The isostatic gravity map from the WGM2012 model (Bonvalot et al., 2012) with a 50 km wide lowpass filter applied. The black dashed line outlines the region with a low isostatic gravity anomaly, which is used for comparison purposes. (b) Shear-wave velocity map at the depth of 8 km. The black dashed line is taken from (a). (c, d) Two vertical cross-sections with strata information derived from Pivnik et al. (1998). Locations of the cross-sections are shown as red lines crossing the low gravity anomaly in (a). Note that the mismatch between our Vs model and the seismic reflection profiles is mainly caused by the horizontal smoothing introduced during seismic tomography.

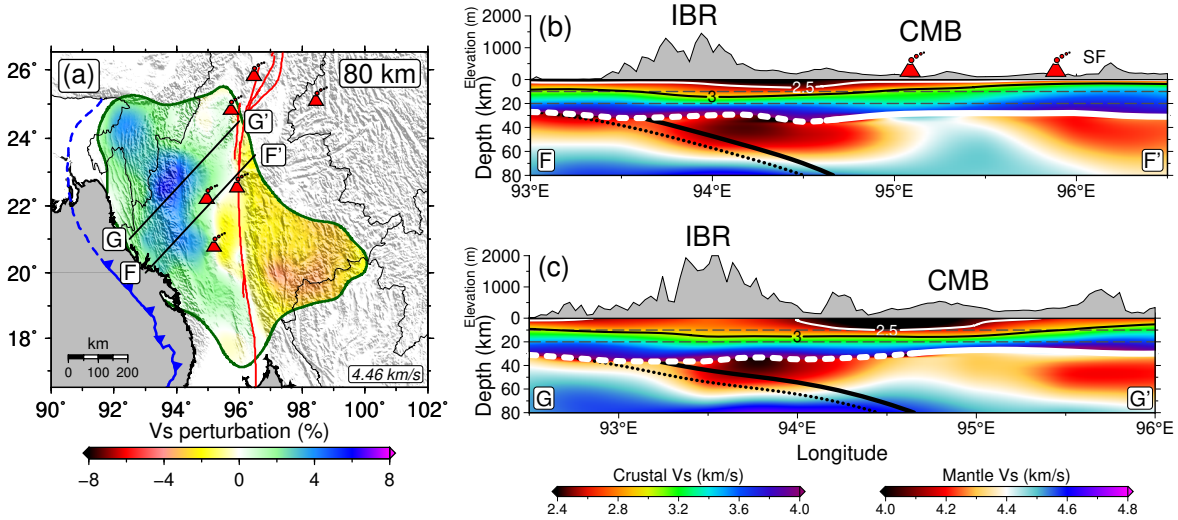

Fig. S4 Two supplementary SW-NE trending vertical cross-sections (b) FF' and (c) GG', along with their locations given in (a). See Fig. 7 for the meanings of different lines and abbreviations.

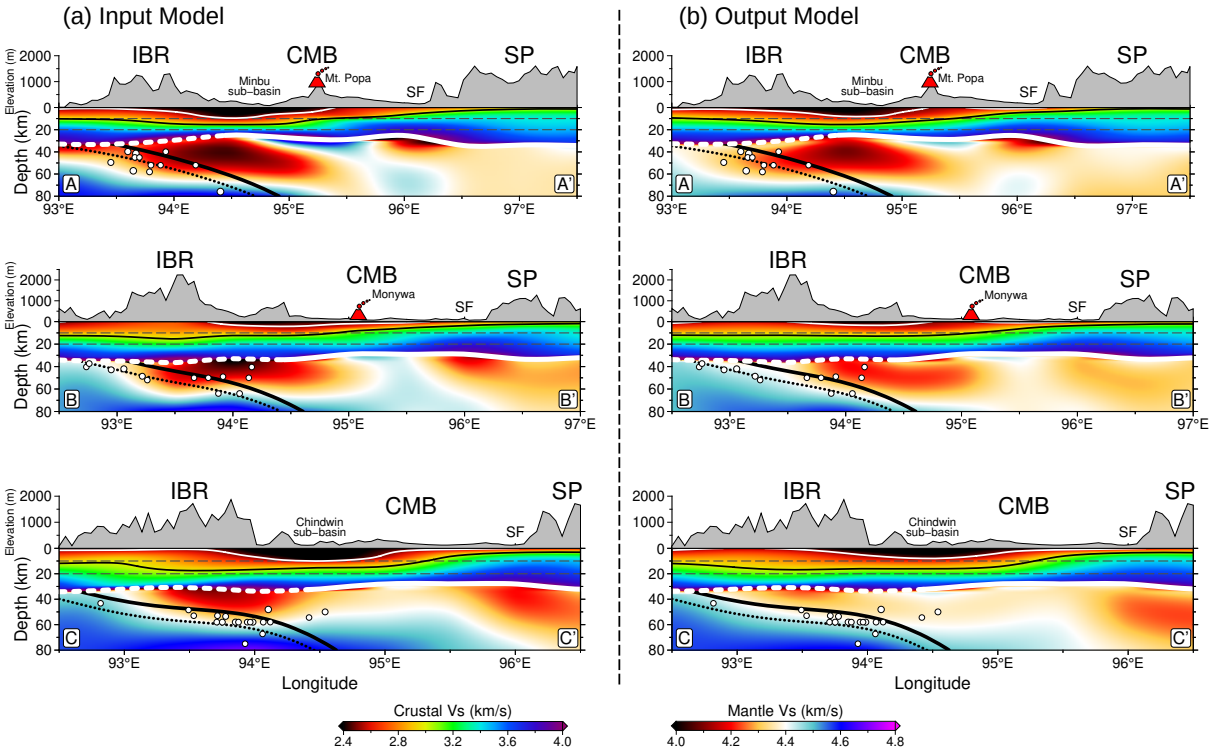

Fig. S5 Recovery resolution tests. (a) The input model (inverted velocity model) along three vertical cross-sections with locations shown in Fig. 6f. (b) The resulted shear-wave velocity model along the same vertical cross-sections in (a). The meanings of different lines are the same as in Fig. 7.

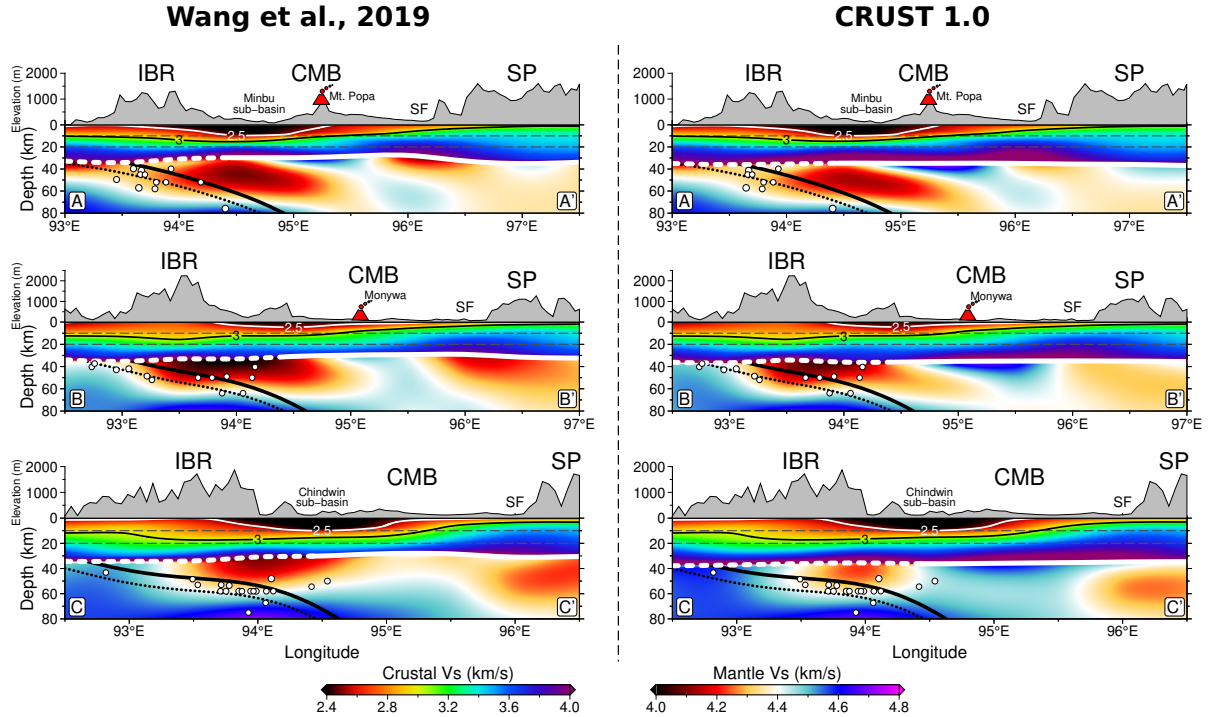

Fig. S6 Comparison of vertical profiles AA'–CC' based on the inversion with different prior Moho depths. Locations of the profiles are shown in Fig. 6f. The left column shows the inversion results when Moho depths from Wang et al. (2019) are used, while the right column shows the results when Moho depths from CRUST1.0 (Laske et al., 2013) are used. A free searching range of ±2 km is assigned to the prior Moho depth in the inversion. The meanings of different lines and symbols are the same as in Fig. 7.

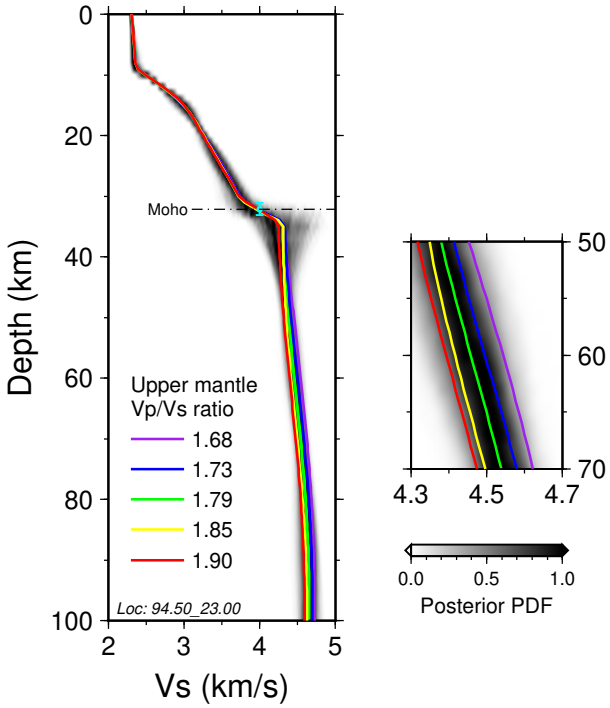

Fig. S7 Inversion tests using different Vp/Vs ratios in the upper mantle for the grid node (94.50°E, 23.00°N). Background color denotes the probability density function (PDF) of the inversion using a Vp/Vs ratio of 1.79 in the upper mantle. The dot-dash line represents the averaged Moho depth of all the accepted models, and the cyan error bar denotes its uncertainty. The right figure shows a zoom-in view between 50 and 70 km depth.

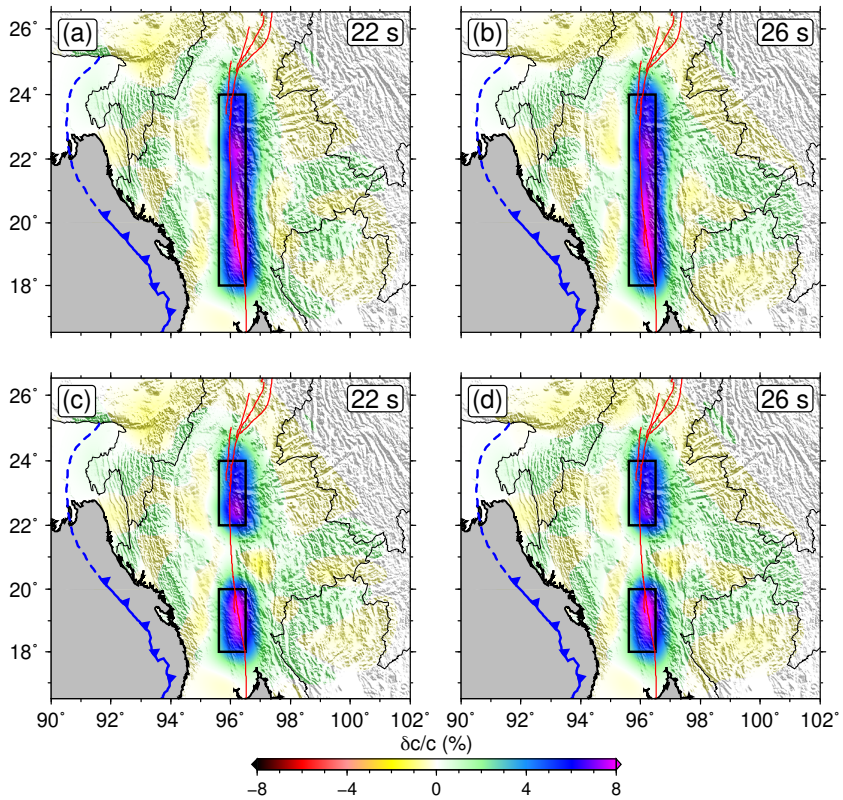

Fig. S8 Recovery tests of the high-velocity anomaly along the Sagaing fault at 22 and 26 s period. Black rectangles outline the spatial distribution of the input high velocities (+8%). (a, b) A single continuous N-S high-velocity anomaly along the SF. (c, d) Two separated N-S high-velocity anomalies along the SF.

Reference

Bonvalot, S., Balmino, G., Briais, A., Kuhn, M., Peyrefitte, A., Vales, N., Biancale, R., Gabalda, G., Reinquin, F., Sarrailh, M., 2012. World gravity map. Commission for the Geological Map of the World. Eds. BGI-CGMW-CNES-IRD, Paris.

Laske, G., Masters, G., Ma, Z., Pasyanos, M., 2013. Update on CRUST1.0 - A 1-degree global model of Earth's crust. Geophys. Res. Abstracts, pp. Abstract EGU2013-2658.

Pivnik, D.A., Nahm, J., Tucker, R.S., Smith, G.O., Nyein, K., Nyunt, M., Maung, P.H., 1998. Polyphase Deformation in a Fore-Arc/Back-Arc Basin, Salin Subbasin, Myanmar (Burma)1. AAPG Bulletin 82, 1837-1856.

Wang, X., Wei, S., Wang, Y., Maung Maung, P., Hubbard, J., Banerjee, P., Huang, B.-S., Moe Oo, K., Bodin, T., Foster, A., Almeida, R., 2019. A 3-D Shear Wave Velocity Model for Myanmar Region. Journal of Geophysical Research: Solid Earth 124, 504-526.